Food Hydrocolloids 129 (2022) 107623

Contents lists available at ScienceDirect

Food Hydrocolloids

journal homepage: www.elsevier.com/locate/foodhyd

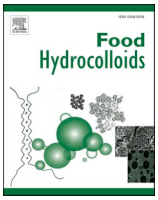

Konjac glucomannan decreases metabolite release of a plant-based fishball analogue during *in vitro* digestion by affecting amino acid and carbohydrate metabolic pathways

Xinli Ran [a], Zhixin Yang [b], Yingfeng Chen [b], Hongshun Yang [a,b,*]

[a] Department of Food Science & Technology, National University of Singapore, Singapore, 117542, Singapore
[b] National University of Singapore (Suzhou) Research Institute, 377 Lin Quan Street, Suzhou Industrial Park, Suzhou, Jiangsu, 215123, PR China

ARTICLE INFO

Keywords:
Nuclear magnetic resonance (NMR)
Food metabolomics
Polysaccharide
Viscosity
Viscoelasticity
Plant-based protein

ABSTRACT

Konjac glucomannan (KGM) provides a sense of fullness by delaying physiological processes related to food digestion, which helps weight management and cholesterol maintenance. This study assessed the influence of KGM on the digestive performance of a plant-based fishball (PFB) analogue during *in vitro* digestion via nuclear magnetic resonance (NMR) spectroscopy and rheological measurements. A total of 27 metabolites were identified, such as amino acids, sterols, saccharides, and fatty acids. Moreover, KGM generally decreased the released amino acids, glucose, and fatty acids. It is possible because KGM affected the metabolic pathways of amino acids and carbohydrates, based on Kyoto Encyclopedia of Genes and Genomes (KEGG) pathway analysis. Furthermore, PFB6.5 (PFB with 6.5% of KGM) digesta exhibited significantly higher yield stress τ_0 (28.0 Pa), consistency coefficient K (46.25 Pa·S^n), and viscoelasticity G_0* (749 Pa) than PFB3.5 (9.2 Pa, 14.66 Pa·S^n, 188 Pa). Besides, surface morphology indicated that fishball digesta became more porous, dissociative, and fragmented than PFB, revealing KGM reduced the breakdown of proteins. In conclusion, KGM prolonged the digestion and decreased metabolite release of PFB, which may help control appetite and reduce postprandial blood glucose levels.

1. Introduction

Konjac glucomannan (KGM) is recognized as a long-chain polysaccharide that contains D-mannose and D-glucose linked by β-1,4 linkages (Yuan, Xu, Cui, & Wang, 2019). KGM is a non-digestible polysaccharide in human gastrointestinal tracts as amylase in human saliva and pancreas cannot break down the β-1,4 linkages within KGM (Devaraj, Reddy, & Xu, 2019). However, KGM could be fermented by intestinal bacteria (Devaraj et al., 2019). It has been widely applied as a food additive to improve the physicochemical properties of foods and develop healthy food products. For instance, KGM was utilized in restructured seafood products (Herranz, Tovar, Solo-de-Zaldívar, & Borderias, 2012), fish surimi (Herranz, Tovar, Borderias, & Moreno, 2013), and cheese pie (Marcano, Hernando, & Fiszman, 2015) to promote gel qualities; in processed cheese (da Silva, de Souza Ferreira, Bruschi, Britten, & Matumoto-Pintro, 2016; Dai, Jiang, Shah, & Corke, 2019), meat products (Jimenez-Colmenero, Cofrades, Herrero, Solas, & Ruiz-Capillas, 2013), and mayonnaise (Li, Wang, Jin, Zhou, & Li, 2014), as a fat replacer. The significant contribution of KGM to health includes weight loss, the maintenance of blood glucose and cholesterol level, the enhancement of intestinal motion, and the improvement of immune system function (Devaraj et al., 2019). These health benefits of KGM are intensively associated with its ability to provide a sense of satiety as it can form a highly viscous and gel-like matrix during digestion, which prolongs gastric emptying and reduce subsequent energy intake (Marcano et al., 2015). Besides, KGM, like other dietary fibers, can absorb a large amount of water and enhance stool bulk, thereby enabling the laxative effect (Chen, Cheng, Liu, Liu, & Wu, 2006).

Theoretically, physiological behavior related to food digestion and absorption should be evaluated *in vivo* on humans; nevertheless, *in vitro* digestion is generally considered as an alternative technique for *in vivo* digestion, as it is relatively rapid, straightforward, low labor, low cost, and importantly, no ethical restriction (Shang et al., 2020). Furthermore, the metabolite release and its profiling after digestion are helpful to understand the functional and nutritional properties of food products. Several analytical technologies, including mass spectroscopy (MS), high-performance liquid chromatography (HPLC), nuclear magnetic resonance (NMR) spectroscopy, can be used for identifying metabolites

* Corresponding author. Department of Food Science & Technology, National University of Singapore, Singapore 117542, Singapore.
E-mail address: fstynghs@nus.edu.sg (H. Yang).

https://doi.org/10.1016/j.foodhyd.2022.107623
Received 31 December 2021; Received in revised form 21 February 2022; Accepted 24 February 2022
Available online 28 February 2022

during the *in vitro* digestion (Escudero, Sentandreu, & Toldra, 2010; Ferranti et al., 2014). The NMR-based metabolomic is advantageous among these methods for it provides qualitative and quantitative measurement without destructive nature and allows metabolites to be identified simultaneously (Lou, Zhai, & Yang, 2021). The application of NMR metabolomic to metabolic profiling of *in vitro* digestion has been reported to the metabolic identification of freshwater fish soups (Cao et al., 2020), sponge cake (Huang, Zhao, Mao, Chen, & Yang, 2021), and cheese (Piras et al., 2013).

In addition, rheological characteristics can influence the food digestion process as they are associated with the overall breakdown of foods, thereby affecting hydrolysis, transportation, and absorption of nutrients during digestion (Keppler, O'Meara, Bakalis, Fryer, & Bornhorst, 2020; Wu, Dhital, Williams, Chen, & Gidley, 2016). For example, enhancing the viscosity of a food product enables a sense of fullness (Morell, Fiszman, Varela, & Hernando, 2014). The increased viscosity would diminish nutrient absorption and mixing in gastrointestinal tracts, helping to maintain postprandial blood glucose (Bornhorst, Ferrua, Rutherfurd, Heldman, & Singh, 2013; Lentle & Janssen, 2008). Besides, shear-thinning flow and gel-like viscoelastic properties are related to the deformability and volume fraction of materials (Morell et al., 2014), impacting the digestion process. Therefore, it is possible to correlate the variation in viscosity and viscoelasticity to digestive performance and satiety feeling during digestion.

Food products formulated with KGM have been accessible in some Asian and European countries, including noodles, tofu, and pasta products, which are claimed to help control body weight and blood glucose. Although awareness of the health benefits of KGM-related foods is increasing (Zhang, Xie, & Gan, 2005), little research is accessible on the digestive performance and metabolite release of actual food products formulated with KGM.

The objectives of current research were to provide a better understanding of the impact of KGM on the digestive performance and rheological behavior of PFB via the *in vitro* digestion model; to investigate the influence of KGM on metabolite release and metabolic pathways during digestion based on NMR foodomics and KEGG pathway analysis; thereby to provide a foundation for the development of more varieties of plant-based seafood analogues added with KGM.

2. Materials and methods

2.1. Materials

Konjac glucomannan (KGM) was bought at iHerb (Moreno Valley, the U.S.); Soy protein isolate (SPI) was bought at Myprotein (Cheshire, the U.K.); other ingredients such as dietary alkali, sunflower oil, tapioca starch, sea salt, and sucrose were bought at a supermarket located in Singapore; *Itoyori* fish surimi (AA grade 600/800) was bought at Thong Siek Food Industry Pte Ltd, a local food manufacturer in Singapore.

Moreover, α-amylase (EC 3. 2. 1. 1, 10 U/mg) originated from the porcine pancreas, pepsin (EC 3. 4. 23. 134 1, 4177 U/mg) originated from porcine gastric mucosa, pancreatin (EC 232. 468. 9, 96.7 U/mL, based on the enzymatic activity of trypsin) originated from porcine pancreas, bile extract, and other chemicals (analytical grade) were bought at Sigma-Aldrich Pte Ltd located in Singapore.

2.2. Sample preparation

The plant-based fishball analogues (PFB) were prepared according to a previous report (Ran, Lou, Zheng, Gu, & Yang, 2022). The KGM addition level in PFB was 3.5%, 5.0%, 6.5% and 8.0%, respectively. In the current study, PFB3.5 (3.5% KGM addition) and PFB6.5 (6.5% KGM addition) were selected as representative PFBs, as 3.5% was the lowest concentration used while 6.5% was the proper concentration to mimic fishball texture.

To prepare for PFB, SPI (7.0%, w/w) was dissolved in distilled water (30%, v/w) for 0.5 h, followed by adding sucrose (0.5%, w/w), sea salt (1.5%, w/w), dietary alkali (0.5%, w/w), and sunflower oil (3.5%, v/w). The mixtures were well mixed (5 min) in a blender (Panasonic, Japan). Ice was added afterwards to prevent heat generation while stirring (53.5% added in PFB3.5 and 50.5% added in PFB6.5, respectively). Afterwards, KGM (3.5% and 6.5%, respectively) was added to the blender slowly while blending. The deacetylation degree for PFB3.5 and PFB6.5 mixture was 35.6% and 61.1%, respectively. The mixed paste was manually made into a round shape (30.0 ± 1.0 g) and cooked (90 °C, 30 min) with a water bath to obtain PFB samples. The deacetylation degree for PFB3.5 and PFB6.5 mixture was measured following Hu et al. (2019), and the results were 35.6% and 61.1%, respectively. To prepare for FB, the *Itoyori* surimi (88.5%, w/w), sea salt (1.5%, w/w), and starch (5.0%, w/w) were mixed with distilled water (5.0%, v/w) in a food processor for 5 min. The subsequent preparation was the same as the preparation of PFB samples.

2.3. In vitro digestion

A three-phase model was applied for the *in vitro* digestion of FB and PFB. The method was illuminated in previous references (Huang et al., 2021; Minekus et al., 2014). The preparation for stock solutions of simulated digestive fluids is shown in Table S1, including the SSF (simulated salivary fluid), SGF (simulated gastric fluid), and SIF (simulated intestinal fluid). Before digestion, samples were minced using a pestle and mortar for 15 min. The minced samples were preheated at a water bath to 37 °C before digestion.

During simulated oral stage (pH 7.0), 8.0 mL α-amylase solution (actual activity of enzyme = 75 U/mL) made up using SSF and 50 μL $CaCl_2$ (0.3 mol/L) were mixed with 1.95 mL deionized water to obtain a total volume of 10 mL. Afterwards, 30 μL HCl (1 mol/L) was used to correct pH value. The resulting mixture was prewarmed at a water bath to 37 °C, followed by adding 10 g of the minced PFB or FB sample and incubating at 37 °C with shaking (200 rpm) for 2 min.

During simulated gastric stage (pH 3.0), 16 mL pepsin solution (actual activity of enzyme = 2000 U/mL) made up using SGF, 10 μL $CaCl_2$ (0.3 mol/L), and 1.30 mL HCl (1 mol/L) were mixed with 2.69 mL deionized water and then prewarmed to 37 °C. Afterwards, the mixture was combined with the oral stage outcome and digested at the water bath (37 °C) at 200 rpm shaking for 2 h.

During simulated intestinal digestion (pH 7.0), 32 mL pancreatin solution (actual activity of enzyme = 100 U/mL) made up using SIF, 80 μL $CaCl_2$ (0.3 mol/L), 0.3536 g bile, 800 μL NaOH (1 mol/L), and 6.96 mL deionized water were mixed with 160 μL amyloglucosidase and prewarmed. Then, the resulting mixture was combined with the gastric stage outcome and digested at the water bath (37 °C) at 200 rpm shaking for 2 h. The intestinal phase outcome was heated immediately in boiling water to finish the digestion reaction.

2.4. NMR spectroscopy

For samples before *in vitro* digestion, samples were minced and extracted with trichloroacetic acid (TCA) solution (7.5%, v/v), with the ratio of minced sample to the solution being 1:2. Afterwards, the mixture was filtered via three-layer filter paper, followed by centrifugation for 10 min (12000×*g*, 4 °C) to separate sediments. The supernatants after centrifugation were filtered using 0.22 μm microporous membranes and freeze-dried for subsequent NMR tests. For PFB and FB digesta, the supernatants after *in vitro* digestion were collected and centrifuged for 5 min (5000×*g*, 4 °C), followed by filtration via 0.22 μm microporous membrane and then freeze-drying for further analysis. The digestive enzymes used for *in vitro* digestion were separately dissolved with water to the same concentration as those during digestion to obtain their NMR spectra.

The samples (50 mg) after freeze-drying were mixed with 1.5 mL D_2O (deuterated water) with 0.01% TSP (sodium 3-trimethylsilyl

[2,2,3,3-d4] propionate) (Chen, Zhao, Wu, He, & Yang, 2020), followed by centrifugation for 10 min (12000×*g*, 4 °C). Afterwards, the obtained supernatants (600 μL) were pipetted to NMR tubes (5 mm in diameter). The NMR samples were measured with Bruker DRX-500 NMR spectrometer (Rheinstten, Germany) at 500.23 MHz. The spectral width of the resulting ^{1}H spectra was within 10.0 ppm at a standard NOSEY setting (noesypr1d). Moreover, the 1D spectra were collected after 128 scans, and a 90° pulse length was automatically corrected via a pulse calculation test (pulse cal) (Chen et al., 2019). To further identify metabolic substances, a standard 2D ^{1}H–^{13}C HSQC (heteronuclear single quantum coherence spectroscopy) of representative samples was also carried out. The spectral width of ^{13}C spectra in F1 channel was within 180.0 ppm, while that of ^{1}H spectra in F2 channel was within 10.0 ppm (Chen et al., 2020).

The baseline adjustment and phase correction of the NMR spectra of PFB and FB samples were performed using MestReNova 14.2.0 (Mestrelab Research, S.L., Spain). Metabolite identification was conducted by cooperatively analyzing the 1D 1H and 2D 1H–13C spectra. Chemical shifts were assigned through Human Metabolome Database (https://hmdb.ca/) and previous studies (Huang et al., 2021; Zhao, Chen, Wu, He, & Yang, 2020). The spectrum peaks between 0 and 10.0 ppm were normalized and integrated to the TSP peak area located at 0.0 ppm through MestReNova 14.2.0. The deuterium oxide region ranging from 4.75 to 4.82 ppm was cut from the original spectra because it may contain signals from water molecules. The width of each region bucket was 0.02 ppm. The region buckets were separated from the normalized spectra, and the dataset after binning was obtained and used for further multivariate analysis.

The resulting binned datasets were imported to SIMCA13.0 software (Umetrics, Sweden) for principal component analyses (PCA). A further helpful model, OPLS-DA (Orthogonal projection to latent structures-discriminant analyses), was also performed based on PCA results. The effectiveness of PCA and OPLS-DA models was assessed via R^2X and Q^2 values. Besides, the analyses of VIP scores (variable importance in projection) were conducted for screening significant metabolites. Furthermore, the MetaboAnalyst5.0 (https://www.metaboanalyst.ca/) was applied to perform the enrichment analysis of identified metabolites after *in vitro* digestion, based on KEGG human metabolic pathways.

2.5. Apparent viscosity and viscoelasticity of digesta

The apparent viscosity and viscoelasticity of *in vitro* digesta were determined using a rheometer with stress control (MCR102, Anton Paar, Austria). A stainless parallel plate (25 mm in diameter) was utilized, and the distance between the plate and sample holder was set as 1.0 mm during the test. For FB and PFB samples before digestion, the samples were prepared by grinding for 15 min with a mortar and pestle. Samples were equilibrated for 5 min before measurements (37 °C). Each sample was tested in triplicate. Three measurements were performed: (1) A strain sweep test was first conducted at 6.28 rad/s (angular frequency) to acquire LVER (linear viscoelastic region) for each sample; (2) A frequency sweep measurement was conducted with a frequency between 0.1 and 100 rad/s within the LVER determined by strain sweep test; (3) A steady shear flow measurement was also conducted with a shear rate between 0.01 and 10 s^{-1}.

2.6. Surface morphology

The surface microstructure of FB and PFB samples was visualized under the Field Emission Scanning Electron Microscope (FESEM, JEOL JSM-6701F). After freeze-drying, the samples were sprayed to a double-sided carbon adhesive tape attached to an aluminum plate, followed by coating using a filmy gold (Huang et al., 2021). The samples were observed under 3 kV accelerating voltage. A magnification of 5000 × was applied to observe the surface morphology of each sample.

2.7. Statistical analyses

All the experiments were conducted in triplicates independently. The resulting data were recorded as mean values ± standard deviations. The Duncan's test and a one-way ANOVA were applied to evaluate statistical significance by SPSS20.0 software (IBM Corp., Armonk, NY, USA). The *P*-value was obtained to reveal statistically significant differences ($P < 0.05$) for the data.

3. Results and discussions

3.1. Determination and comparison of metabolites

The metabolites in the digesta were identified via the NMR ^{1}H spectra profiling. Fig. 1 (I - III) shows the corresponding NMR spectrum for FB, PFB3.5, and PFB6.5 after *in vitro* digestion. While FB had a slightly different chemical shift spectrum with PFB3.5 and PFB6.5, they presented a similar overall profile having different signal intensities, indicating the metabolite profiles of FB and PFB after *in vitro* digestion were close while different content of individual metabolites. The ^{1}H peaks were primarily located at 0.5–5.5 ppm, where the metabolites typically include saccharides, aliphatic acids, and amino acids (Chen et al., 2019). These observations agreed with previous studies showing that processed fish products and plant-based meat analogues contain polysaccharides (starch, sugar, and dietary fibre), amino acids, and fatty acids after *in vitro* digestion (Cao et al., 2020; Van Vliet et al., 2021). Furthermore, the qualitative determination of metabolites after *in vitro* digestion was conducted based on ^{1}H 1D binned area datasets and 2D ^{1}H–^{13}C spectra. A total of 27 metabolic compounds were identified in FB and representative PFB samples after *in vitro* digestion, including amino acids, carbohydrates, fatty acids, and sterol (Fig. 1, Table 1, and Table S2). The ^{1}H peaks at around 0.5–0.75 ppm were assigned as sterols (Chen et al., 2020), which are metabolites from plants and play an essential role in health maintenance (Kim & Van Ta, 2012). Furthermore, most amino acids and fatty acids (linoleic and palmitic aid) were assigned to the region ranging from 0.75 to 4.0 ppm of ^{1}H spectra (Lou et al., 2021). The peaks at 4.0–5.5 ppm were generally assigned to soluble sugars such as sucrose, β-D-glucose, α-D-glucose, and D-maltose (Zhao et al., 2020). Peaks on the ^{1}H spectrum from 6.5 to 8.0 ppm indicated the presence of phenylalanine and tryptophan (Huang et al., 2021). Overall, the amino acids were primary composites after *in vitro* digestion of FB and PFB (PFB3.5 and PFB6.5), followed by saccharides such as fructose, maltose, and glucose. These metabolites in FB were attributed to the enzymatic hydrolysis of main ingredients, including fish protein and starch. The presence of these metabolites in PFB was because of the enzymatic hydrolysis of ingredients such as soy protein and sugar during simulated digestion.

3.2. Principal component analyses

Principal component analyses (PCA) were applied to investigate the influence of KGM on the metabolic changes of PFB after *in vitro* digestion, providing an overview of metabolic changes by screening primary metabolites (Wu, Zhao, Lai, & Yang, 2021). As shown in Fig. 2A, the first three principal components (PCs) explained 91.3% (PC1: 60.5%, PC2: 20.4%, PC3:10.4%) of total data from group I (FB), group II (PFB3.5), and group III (PFB6.5). The three groups were separated into three clusters on scores plotting (Fig. 2B). Additionally, the metabolic profile of group I (FB) was negatively influenced by PC1, while that of group II and group III (PFB3.5 and PFB6.5) was positively influenced by PC1 (Table S3). The separation of PFB3.5 from PFB6.5 indicated that the KGM influenced the metabolite release of PFB after *in vitro* digestion, depending on KGM addition levels. A loading plotting was performed for distinguishing those metabolites contributing to variable separations (Fig. 2C). For instance, glutamine, serine, and arginine positively correlated with FB (group I); meantime, sterol, valine, oleic acid, and

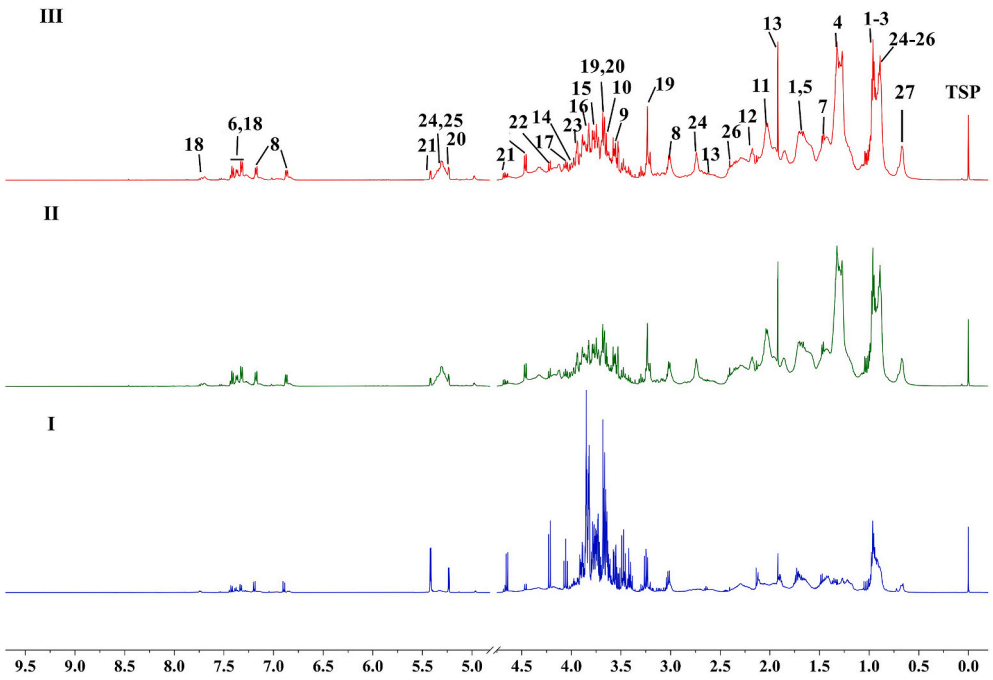

Fig. 1. The NMR ^{1}H spectra of the fishball (FB) and plant-based fishball (PFB) analogues after *in vitro* digestion. Note: group I-III represent FB, PFB3.5 (PFB at 3.5% konjac glucomannan addition), and PFB6.5 (PFB at 6.5% konjac glucomannan addition), respectively.

Table 1
Identified metabolites in plant-based fishball analogue at 6.5% konjac glucomannan (KGM) addition after *in vitro* digestion.

	Metabolites	^{1}H chemical shifts (ppm)
1	Leucine	3.74 (m), 1.71 (m), 0.97 (t), 0.90 (m)
2	Isoleucine	3.57(d); 1.98(m); 1.47(m); 1.02(d); 0.95(t)
3	Valine	3.63(d); 2.27(m); 1.04(d); 0.99(d)
4	Threonine	4.20(m); 3.57(d); 1.32(d)
5	Lysine	3.71(m); 3.01(t); 1.71(m); 1.45(m)
6	Phenylalanine	7.42(m); 7.37(m); 7.33(d); 3.93(m); 3.23(m)
7	Alanine	3.76(q); 1.47(d)
8	Tyrosine	7.18(d); 6.88(m); 3.88(m); 3.01(d)
9	Glycine	3.54(s)
10	Glutamine	3.65(t); 2.45(m); 2.15(m)
11	Glutamate	3.71(m); 2.28(m); 2.04(m)
12	γ-aminobutyric acid	3.01(t); 2.19(t); 1.92(s)
13	Aspartic acid	3.82(m); 2.86(m); 2.65 (m)
14	Asparagine	3.99(dd); 2.88(dd)
15	Arginine	3.75(t); 3.23(t); 1.71(m)
16	Serine	3.94(m); 3.83(t)
17	Proline	4.07(m); 2.29(m); 2.03(d)
18	Tryptophan	7.73(d); 7.53(d); 7.32(d); 7.26(m); 7.18(m); 4.04(t); 3.47(t), 3.28(q)
19	β-D-Glucose	4.47(d); 3.24(m); 3.39(m); 3.46(m); 3.52(m); 3.68 (m)
20	α-D-Glucose	5.24(d); 3.82(m); 3.78(m); 3.68(m); 3.48(m)
21	D-Maltose	5.42(d); 5.24(d); 4.66(d); 3.92(m); 3.89(m); 3.82(m); 3.76(m); 3.70(m); 3.68(m); 3.53(t); 3.42(t); 3.30(t); 3.25(t)
22	Sucrose	4.21(d); .06(t); 3.94(m); 3.55 (m); 3.53(t); 3.48(t); 3.42 (t);
23	β-D-Fructose	4.02(d); 4.00(m); 3.94(m); 3.79(d); 3.87(m)
24	Linoleic acid	5.37(m); 2.74(m); 2.40(t); 2.03(d); 1.66 (m); 1.28(m); 0.89(t)
25	Oleic acid	5.34 (m); 2.40(t); 2.03(d); 1.65(m); 1.28(m); 0.89(t)
26	Palmitic acid	2.40(t); 1.65(m); 1.28(m); 0.89(t)
27	Sterol	0.65(d)

β-D-Glucose showed a positive correlation with PFB (group II and III). Plant sterols (phytosterols) are abundant in vegetable oils (32.3–67.7%), nuts (61.9–86.7%), legumes (13.2–34.7%), and cereals (27.2–62.4%), which predominantly exist as β-Sitosterol (Kim and Van Ta, 2012). Sterols are metabolites from plant-based sources and play an essential role in maintaining health (Kim and Van Ta, 2012).

3.3. Comparison of metabolite release within pairwise groups

A further powerful statistical modeling tool, the OPLS-DA model, was applied to assess the separations within the two paired groups: I vs. III (FB vs. PFB6.5), II vs. III (PFB3.5 vs. PFB6.5). The comparison between FB and PFB6.5 (the representative plant-based fishball analogue) was performed to evaluate the difference in metabolite release after digestion between fishball and plant-based fishball analogues. Meantime, the comparison between PFB3.5 and PFB6.5 was performed to evaluate the impact of KGM on the metabolite release of plant-based fishball analogues.

The established OPLS-DA model well interpreted and predicted the data with a high R^2 (0.99 > 0.7) and Q^2 (0.98 > 0.5), respectively (Fig. 3A1). Moreover, groups I and III (FB and PFB6.5) were significantly divided on the score plotting (Fig. 3B1), revealing a different metabolic change between fishball and plant-based fishball analogue. Besides, a loading S-line plot was conducted to determine the significant metabolites leading to the differences within the paired group (Zhao et al., 2020). Upward and downward peaks represent the relative content of specific metabolites was enhanced and reduced in the second group when compared with the first group. Furthermore, the color-coated line indicates metabolite significance within the pairwise group; a more red-coded line indicates more noticeable differences (Wu et al., 2021).

The potential discriminative metabolites were identified based on the OPLS-DA S-line plotting (Fig. 3C1). After *in vitro* digestion, PFB6.5 had a higher content of threonine, glutamate, β-D-Glucose, sterol, oleic acid, and palmitic acid, while FB possessed a higher amount of glutamine, arginine, aspartic acid, proline, sucrose, maltose, and α-D-glucose. The contribution of specific metabolites to the differentiation was assessed via variable importance for the projection (VIP). Generally, the metabolites with a high VIP score (>1) and low coefficient values ($P < 0.05$) were selected as significant contributors for inter-group differentiation (Zhao et al., 2020). Totally nineteen metabolites showed a statistically significant difference between FB and PFB6.5 (Table S5), such as β-D-glucose, D-maltose, α-D-glucose, sucrose, glutamine, serine,

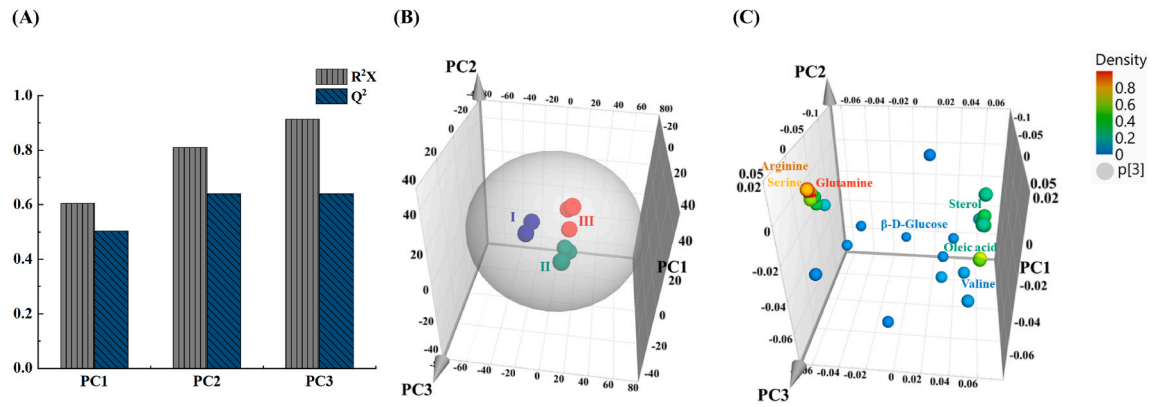

Fig. 2. The principal component analysis (PCA) for fishball (FB) and plant-based fishball analogues (PFB). (A) Fitting summary for PCA model; (B) The 3D scores plotting of PCA; (C) The 3D loading plotting of PCA. Note: group I, II, and III represent FB, PFB3.5 (PFB at 3.5% konjac glucomannan addition), and PFB6.5 (PFB at 6.5% konjac glucomannan addition), respectively.

threonine, sterol, and so forth. The difference in metabolite release between fishball and plant-based fishball was understandable because of the difference in main ingredients of FB (fish surimi and starch) and PFB (soy protein and KGM).

To further understand the effect of KGM on the metabolite release of plant-based fishball analogue, the OPLS-DA model was also performed within pairwise groups II and III (PFB3.5 and PFB6.5). As shown in Fig. 3A2, the first component (PC1) explained 84.1% of data, and the Q^2 of 0.74 showed an excellent fitness of the OPLS-DA model. Group II (PFB3.5) and III (PFB6.5) showed a good separation (Fig. 3B2), indicating that KGM would affect the metabolite release after *in vitro* digestion of PFB, depending on KGM addition concentration. Furthermore, the S-line plotting showed that the higher KGM addition (PFB6.5) decreased the release of linoleic acid, leucine, threonine, palmitic acid, tyrosine, glycine, sucrose, α-D-glucose, oleic acid, and phenylalanine (Fig. 3C2). Significant metabolites contributing to the separation were screened based on a coefficient test and VIP scores. Results showed that eight metabolites were considered as the significant substances ($P < 0.05$, VIP >1) (Table S6), including phenylalanine, tryptophan, oleic acid, linoleic acid, β-D-Glucose, valine, α-D-Glucose, and leucine. Possibly, KGM intervened in the metabolic pathways during *in vitro* digestion of PFB, which would be further illuminated in part 3.6.

3.4. Apparent viscosity and viscoelasticity of digesta

The digestion process in the gastrointestinal tract is associated with the overall breakdown of food products (Huang et al., 2021), which could be indicated by rheological properties, including apparent viscosity and viscoelasticity. Fig. S1 and Fig. 4A show the steady-shear flow curves of FB and PFB after *in vitro* digestion at 37 °C and the resulting apparent viscosity vs. shear rate. The apparent viscosity of FB and PFB after *in vitro* digestion was decreased significantly than the corresponding samples before digestion, which was because digestive enzymes would break down the sample particles in the suspension (Wu et al., 2016). Furthermore, Herschel–Bulkley model was applied to interpret further the steady-shear flow behavior of FB and PFB (Ahmed & Ramaswamy, 2004):

$$\tau = \tau_0 + K \cdot \dot{\gamma}^{n}$$

Where τ presents shear stress (Pa); τ_0 presents yield stress; $\dot{\gamma}$ presents shear rate (S^{-1}); K indicates consistency coefficient (Pa · S^n); n presents flow behavior index. Table 2 summarizes all fitting parameters. The high R^2 and low RMSE values demonstrated an excellent fitness of the model. The yield stress τ_0 denotes the critical stress below which samples exhibit elastic behavior (elastic solid) while above which the samples start to flow (viscous fluid) (Funami, 2011). A higher τ_0 value indicates that more shear stress is needed to break the internal structure to initiate flow, reflecting a stronger and more stable structure.

For samples before digestion, FB and PFB were ground for 15 min with a mortar and pestle. As revealed in Table 2, the FB had significantly lower yield stress τ_0 than PFB before or after *in vitro* digestion, which was because PFB was formulated with KGM (non-digestible fiber), making the structure of PFB harder to be broken by enzymes. Moreover, compared with PFB3.5, PFB6.5 had a significantly higher τ_0 value (78.41 and 28.02 Pa before and after digestion) either before or after digestion. It is possible that KGM entrapped SPI chains, thus reducing the site for the enzymatic reaction, protecting proteins and carbohydrates from reacting with digestive enzymes. This observation could be attributed to the physical entanglement effect introduced by KGM (Luo, He, & Lin, 2013), promoting more stable inner structures formed within SPI/KGM system.

The consistency coefficient K provides a measurement of structure consistency, implying the viscosity of samples (Zheng et al., 2020). The K values of FB and PFB decreased significantly after digestion. Meantime, PFB had a higher K value than FB throughout the entire measurements. This observation could be because KGM would provide entangled networks when incorporated with proteins, thus enhancing the molecular interaction and extension strength within the gel network (Iglesias-Otero, Borderías, & Tovar, 2010). Kim, Choi, Kim, and Lim (2015) also indicated that increased intermolecular interactions or entanglements could enhance the consistency coefficient K. Moreover, between two PFB samples, PFB6.5 exhibited a higher K value (46.25 Pa·S^n) than PFB3.5 (14.66 Pa·S^n) after *in vitro* digestion, reflecting a higher KGM addition led to a higher viscosity in PFB digesta. The increased viscosity induced by KGM was also found in cheese pie containing KGM after *in vitro* digestion (Marcano et al., 2015). It has been reported that enhancing the viscosity of digesta could help some physiological responses, including constipation relief and blood glucose control (Lentle et al., 2008). Moreover, studies have shown that polysaccharides help impart the sense of fullness, which is attributed to increasing viscosity, diminishing enzyme action efficacy, and postponing gastric emptying, therefore prolonging intra-gastric satiety signals (Fiszman & Varela, 2013; Morell et al., 2014). Therefore, the significantly increased viscosity induced by KGM could prolong the digestion process of PFB, which might help control blood glucose and cholesterol levels.

The fluid index n is an indicator of overall fluid behavior, where materials with $n < 1$ present shear-thinning behavior, materials with $n > 1$ present shear-thickening behavior, while materials with $n = 1$ present Newtonian behavior (Hayati, Man, Tan, & Aini, 2009). The digesta of all samples exhibited a shear-thinning behavior ($0 < n < 1$), revealing the apparent viscosity decreased with increasing shear rate (Fig. 4A). Similarly, Huang et al. (2021) showed that sponge cake (added

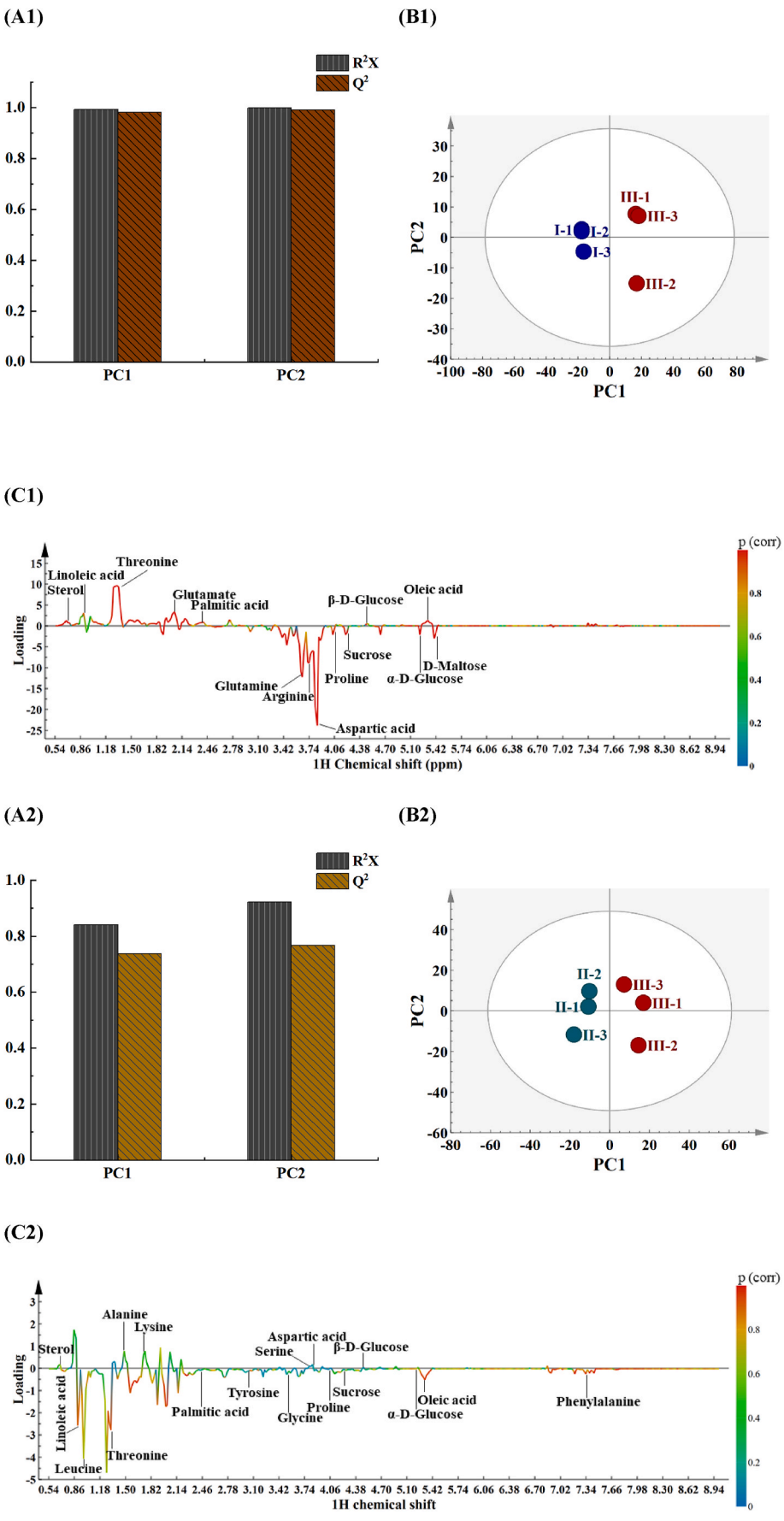

Fig. 3. The OPLS-DA model (Orthogonal projection to latent structures-discriminant analyses for pairwise groups: group I vs. III and group II vs. III. (A1) Fitting summary for OPLS-DA model within the pairwise groups (group I vs. III); (B1) The OPLS-DA scores plotting (group I vs. III); (C1) The OPLS-DA S-line plotting (group I vs. III); (A2) Fitting summary for OPLS-DA model within the pairwise groups (group II vs. III); (B2) The OPLS-DA scores plotting (group II vs. III); (C2) The OPLS-DA S-line plotting (group II vs. III). Note: Group I, II, and III represent FB (fishball), PFB3.5 (PFB at 3.5% konjac glucomannan addition) and PFB6.5 (PFB at 6.5% konjac glucomannan addition), respectively.

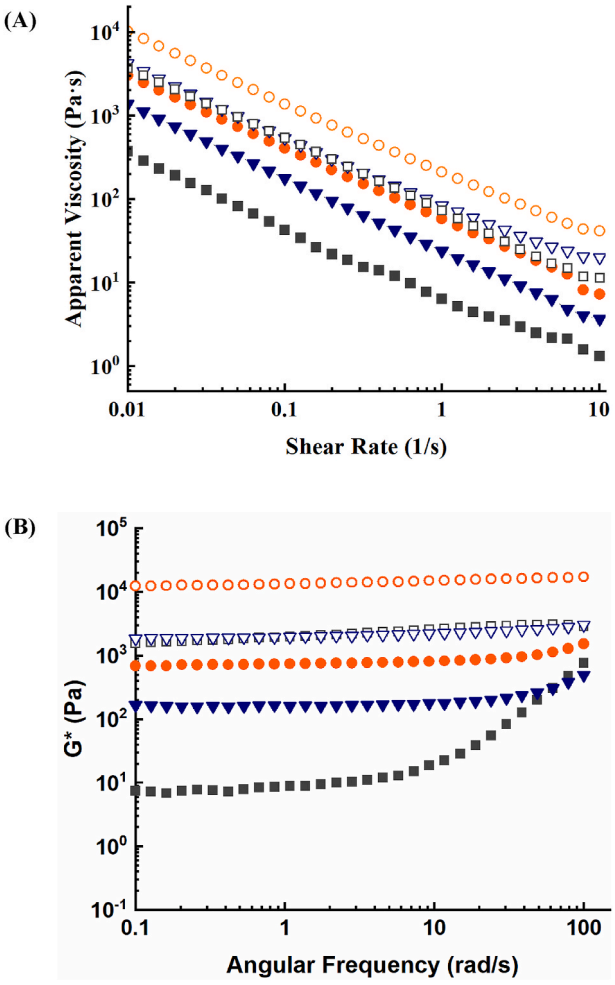

Fig. 4. The apparent viscosity and complex shear modulus G* of fishball (FB) and plant-based fishball (PFB) analogues. (A) The apparent viscosity of FB and PFB before and after *in vitro* digestion at 37 °C; (B) The complex shear modulus G* of FB and PFB before and after *in vitro* digestion at 37 °C. Note: □/■, FB before and after *in vitro* digestion; ▽/▼, PFB at 3.5% konjac glucomannan addition (PFB3.5) before and after *in vitro* digestion; ○/●, PFB at 6.5% konjac glucomannan addition (PFB6.5) before and after *in vitro* digestion.

with fibers) digesta also exhibited a shear-thinning phenomenon after *in vitro* digestion.

Furthermore, complex shear modulus G* (G′ + iG″) was used to describe the overall viscoelastic behavior. Fig. 4B reveals the variations in G* with the angular frequency. Before digestion, the G* values of all samples showed nearly no frequency dependence, indicating relatively stable internal structures. After digestion, the G* of samples (especially FB) showed more frequency dependence, indicating that certain destroys occurred in the internal structures, reducing the number of stable structures in the digesta. Moreover, G_0* values (representing the G* when the frequency was 1 rad/s) could reveal the structural strength (Borderías et al., 2020). As presented in Table 2, the overall viscoelasticity and structure strength after digestion decreased significantly (decreasing in G_0*). The decreased viscoelasticity was attributed to the enzymatic reaction and logical dilution of simulated digestive juices. FB had the lowest viscoelasticity and structure strength (G_0* = 37.0 Pa) after *in vitro* digestion compared with PFB. Between the two PFB samples, PFB at 6.5% KGM addition (PFB6.5) had a significantly higher G_0* value than PFB at 3.5% KGM (PFB3.5) after digestion. The lowest G_0* value of FB demonstrated that FB became less structured, resulting from easier destruction of internal structures. Meantime, the higher G_0* value of PFB6.5 than PFB3.5 indicated that KGM induced more crosslinked

Table 2
The fitting parameters from the Herschel-Bulkley model and complex shear modulus G* before and after *in vitro* digestion.

Fitting parameters	Before digestion			After digestion		
	FB	PFB3.5	PFB6.5	FB	PFB3.5	PFB6.5
Herschel-Bulkley						
τ_0 (Pa)	22.11 ± 0.89^{c}	42.06 ± 0.97^{b}	78.41 ± 0.70^{a}	3.29 ± 0.15^{C}	9.20 ± 0.81^{B}	28.02 ± 0.64^{A}
K (Pa·s^{n})	69.76 ± 0.92^{b}	39.39 ± 0.48^{c}	99.67 ± 0.97^{a}	3.26 ± 0.60^{C}	14.66 ± 0.14^{B}	46.25 ± 0.70^{A}
N	0.51 ± 0.04^{b}	0.57 ± 0.03^{ab}	0.59 ± 0.02^{a}	0.14 ± 0.03^{B}	0.25 ± 0.02^{A}	0.21 ± 0.01^{A}
R^2	0.96	0.99	0.99	0.99	0.99	0.99
RMSE	3.76	3.82	3.38	0.30	0.66	1.28
Complex shear modulus at 1 rad/s						
G_0* (Pa)	1983 ± 29^{c}	2574 ± 46^{b}	10432 ± 92^{a}	37.0 ± 1.2^{C}	188 ± 15^{B}	749 ± 28^{A}

Note: The different lowercase and uppercase alphabets at the same row present a statistically significant difference ($P < 0.05$) among samples before and after *in vitro* digestion, respectively. FB means fishball; PFB3.5 and PFB6.5 means plant-based fishball analogue at 3.5% and 6.5% konjac glucomannan addition, respectively.

and structured network structures, making the PFB granules harder to be interrupted by enzymes during digestion. Similar observations were presented by Marcano et al. (2015), showing that cheese pies added with KGM exhibited a more structured system and higher viscoelasticity after *in vitro* digestion. Similarly, Zheng et al. (2020) reported that adding polysaccharides (xanthan gum) led to more elastic behavior and stronger gels, decreasing the hydrolysis during *in vitro* digestion of starch.

The current study was not to characterize specific rheological behavior but to relate changes in rheological performance to the satiety effect resulting from KGM. Overall, following simulated oral, gastric, and intestinal digestion, PFB at higher KGM addition had significantly ($P < 0.05$) higher apparent viscosity and viscoelasticity, contributing to increasing bulk and thus prolonging the digestion process. Therefore, KGM addition in PFB could delay digestion and decrease metabolite release of PFB, which may help control appetite and postprandial blood glucose level.

3.5. Possible metabolic pathways of PFB during digestion

The difference in the metabolite release and rheological performance of the *in vitro* digesta of PFB3.5, and PFB6.5 could be because KGM influenced the amino acid metabolism, sugar metabolism, and lipid metabolism during digestion. The possible metabolic pathways connected to the digestion process of PFB were visualized via enrichment analyses (Fig. 5A). These pathways included valine, leucine, and isoleucine biosynthesis (amino acid metabolism), D-glutamine and D-glutamate metabolism (amino acid metabolism), unsaturated fatty acid biosynthesis (lipid metabolism), starch and sucrose metabolism (sugar metabolism), nucleotide metabolism, and so forth. Based on *P*-value (<0.05) and enrichment ratio (>15), the top seven pathways were identified as follows: D-glutamine and D-glutamate metabolism; alanine, aspartate and glutamate metabolism; valine, leucine and isoleucine biosynthesis; arginine biosynthesis; phenylalanine, tyrosine, and tryptophan biosynthesis; starch and sucrose metabolism; nitrogen metabolism.

Furthermore, we proposed a schematic illuminating the possible influence of KGM on the metabolic pathways during *in vitro* digestion of PFB (Fig. 5B). The variations in metabolic pathways were mainly divided into amino acid and carbohydrate metabolism. Amino acids resulted from protein (namely SPI) hydrolysis. Compared with PFB3.5 after *in vitro* digestion, PFB6.5 after digestion had a lower proline,

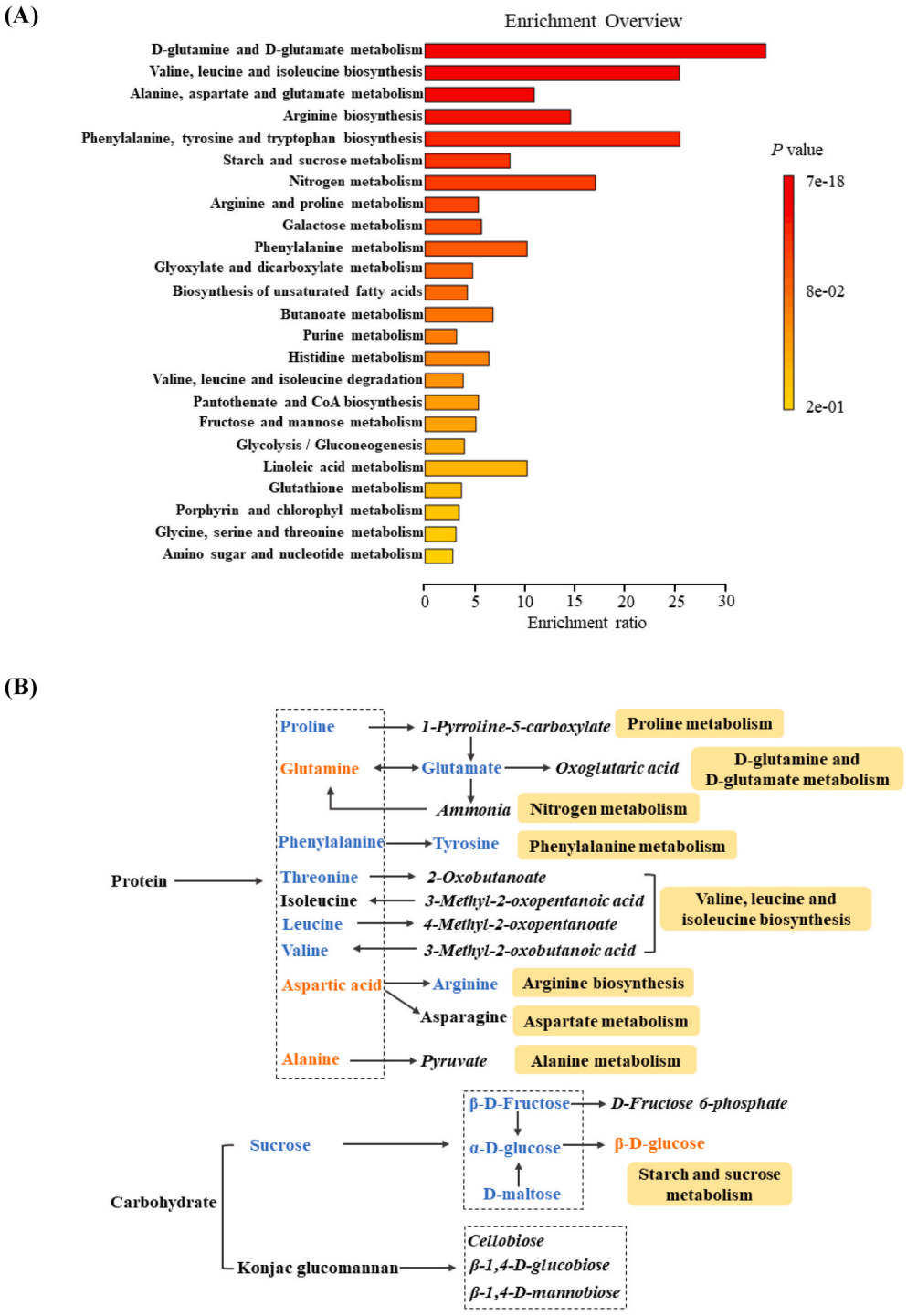

Fig. 5. The enrichment analysis result and proposed schematic for the impact of konjac glucomannan (KGM) on *in vitro* digestion of plant-based fishball analogues (PFB). (A) Enrichment overview of metabolic pathways during *in vitro* digestion process; (B) The influence of KGM on the metabolic changes of PFB after *in vitro* digestion. Note: Metabolites with italic font means those that are not identified in this study; metabolites with blue color means those at decreased content in PFB at 6.5% KGM addition (PFB6.5), compared with PFB at 3.5% KGM addition (PFB3.5); metabolites with orange color means those at increased content in PFB6.5, compared with PFB3.5. (For interpretation of the references to color in this figure legend, the reader is referred to the Web version of this article.)

phenylalanine, tyrosine, threonine, leucine, and valine, while a higher content of glutamine, aspartic acid, and alanine (Fig. 5B, Table S7). This observation indicated that KGM decreased the release of the amino acids, possibly by affecting amino acid metabolism during digestion. A similar observation was also presented by Wang et al. (2021), revealing that KGM greatly influenced the amino acid metabolism of corn starch/KGM composite in the mice model.

Protein would be hydrolyzed into amino acids with enzymatic actions of digestive juices, participating in the metabolism of energies and substances (Wang et al., 2021). Studies have indicated that branched and aromatic amino acids are considerably associated with insulin resistance (Wang et al., 2021). For instance, phenylalanine and tyrosine play a critical part in the process, including protein breakdown and conversion, glycogen synthesis, and so forth (Monirujjaman & Ferdouse, 2014). Würtz et al. (2013) have highlighted the potentials of phenylalanine and tyrosine in diabetes diagnosis. The phenylalanine and tyrosine level were also related to diabetic complications, such as kidney disease, cardioembolic stroke, and cardiovascular issues (Kumar et al., 2012). Excessive phenylalanine and tyrosine may initiate gluconeogenesis and insulin resistance (Wang et al., 2021).

As shown in Table S7, FB generated higher phenylalanine content (4.03 mg/g) and tyrosine (9.53 mg/g) than PFB after *in vitro* digestion. Moreover, PFB6.5 had less phenylalanine content (3.10 mg/g) and tyrosine (3.36 mg/g), compared with PFB3.5 (containing 3.81 mg/g

phenylalanine and 4.43 mg/g tyrosine). This observation revealed that KGM could help decrease the production of phenylalanine and tyrosine. Possibly, KGM intervened in phenylalanine metabolism and phenylalanine, tyrosine and tryptophan biosynthesis during digestion. Noticeably, PFB (containing KGM) exhibited a significantly higher threonine, alanine, glycine, and glutamate content than FB. For instance, the threonine content in FB was 0.25 mg/g, significantly lower than PFB3.5 (35.47 mg/g) and PFB6.5 (34.60 mg/g). Studies have shown that these amino acids are associated with laxative effects and improvement of gastrointestinal motility (Liu et al., 2018; Rodriguez et al., 2013), preventing or reducing constipation. Similarly, Zhang et al. (2021) reported that the intake of KGM could change the content of alanine, arginine, histidine, threonine, glycine, and glutamate in constipated mice. Therefore, PFB might be beneficial to individuals having constipation issues.

Besides the effect on amino acid metabolism, KGM may also impact the carbohydrate metabolism of PFB during the digestion process (Fig. 5B). FB generated a significantly higher content of α-D-glucose, D-maltose, sucrose, and β-D-fructose than two PFB samples after *in vitro* digestion. Besides, PFB6.5 released a lower content of D-maltose, α-D-glucose, and β-D-fructose while a higher content of β-D-glucose, compared with PFB3.5 (Fig. 5B and Table S7). These observations indicated that KGM might reduce the hydrolysis of sucrose and promote the conversion of α-D-glucose to β-D-glucose. It could be because KGM, as a dietary fiber, would increase bulk volume and prolong digestion time (Shah et al., 2015), slowing down the breakdown of carbohydrates and thus decreasing glucose levels. In summary, KGM could decrease the digestive performance of PFB, possibly by intervening in amino acid metabolism and sugar metabolism.

3.6. Schematic model

On the basis of the previous discussions, we presented a potential schematic model illuminating KGM effect on PFB during *in vitro* digestion (Fig. 6). PFB had a significantly higher yield stress τ_0, consistency *K*, and G* than FB after *in vitro* digestion than FB. Moreover, these parameter values of PFB6.5 (6.5% of KGM) were significantly increased compared with PFB3.5, revealing that KGM could increase apparent viscosity and delay the digestion of PFB, which may help maintain body weight and postprandial blood glucose level. KGM is a non-digestible polysaccharide in the stomach. It may entrap SPI chains and thus reduce the site for the enzymatic reaction, protecting proteins and carbohydrates from being reacted with digestive enzymes. As a result, the contents of released amino acids and other metabolites were decreased. FB digesta had a more disconnected and porous structure than PFB digesta; meanwhile, PFB at 6.5% KGM addition had fewer porous and continuous microstructures than PFB at 3.5% KGM addition.

3.7. Validation via surface morphology

The proposed schematic model was validated by visualizing surface microstructure of the digesta. The variation in microstructures of FB and PFB before and after *in vitro* digestion was observed under a scanning electron microscope with 5000× magnification (Fig. 7). Results showed that the FB (dominating with surimi protein) differed in the surface morphology with PFB (dominating with SPI-KGM complex) before or after *in vitro* digestion. The FB before digestion exhibited a flaky and discontinued microstructure (Fig. 7A). In contrast, PFB3.5 and PFB6.5 exhibited a continuous and smooth microstructure (Fig. 7C and E), revealing that FB had a less stable and associative structure than PFB. Besides, PFB6.5 had a more continuous and smoother surface morphology than PFB3.5, which was because the KGM at a higher concentration could strengthen the gel network and thus contribute to a more stable structure (Iglesias-Otero et al., 2010).

After *in vitro* digestion, FB digesta had more dissociative and fragmented than before; meanwhile, FB digesta had more incomplete structures than PFB digesta. For those PFB samples, the continuous structures of digesta were reserved; however, FB3.5 digesta had an

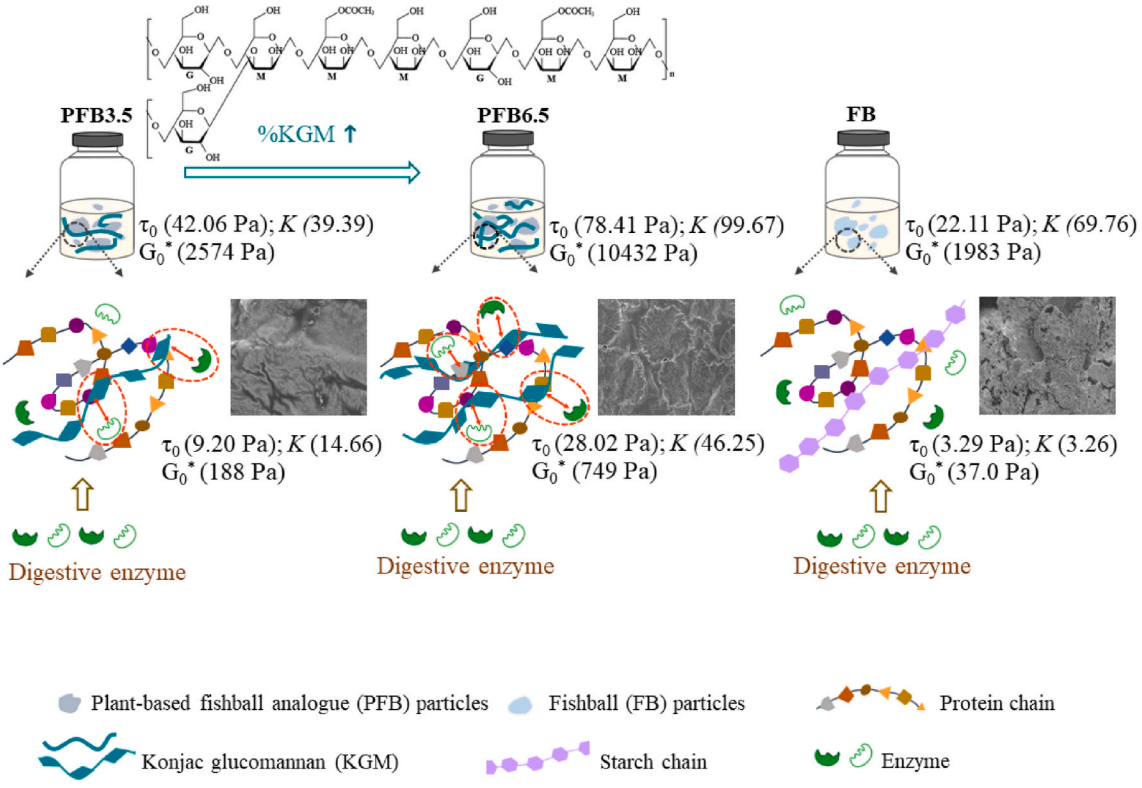

Fig. 6. The proposed schematic model illuminating the effect of konjac glucomannan (KGM) on the *in vitro* digestion of plant-based fishball analogues (PFB). Notes: PFB3.5 and PFB6.5 represent PFB at 3.5% and 6.5% KGM addition, respectively.

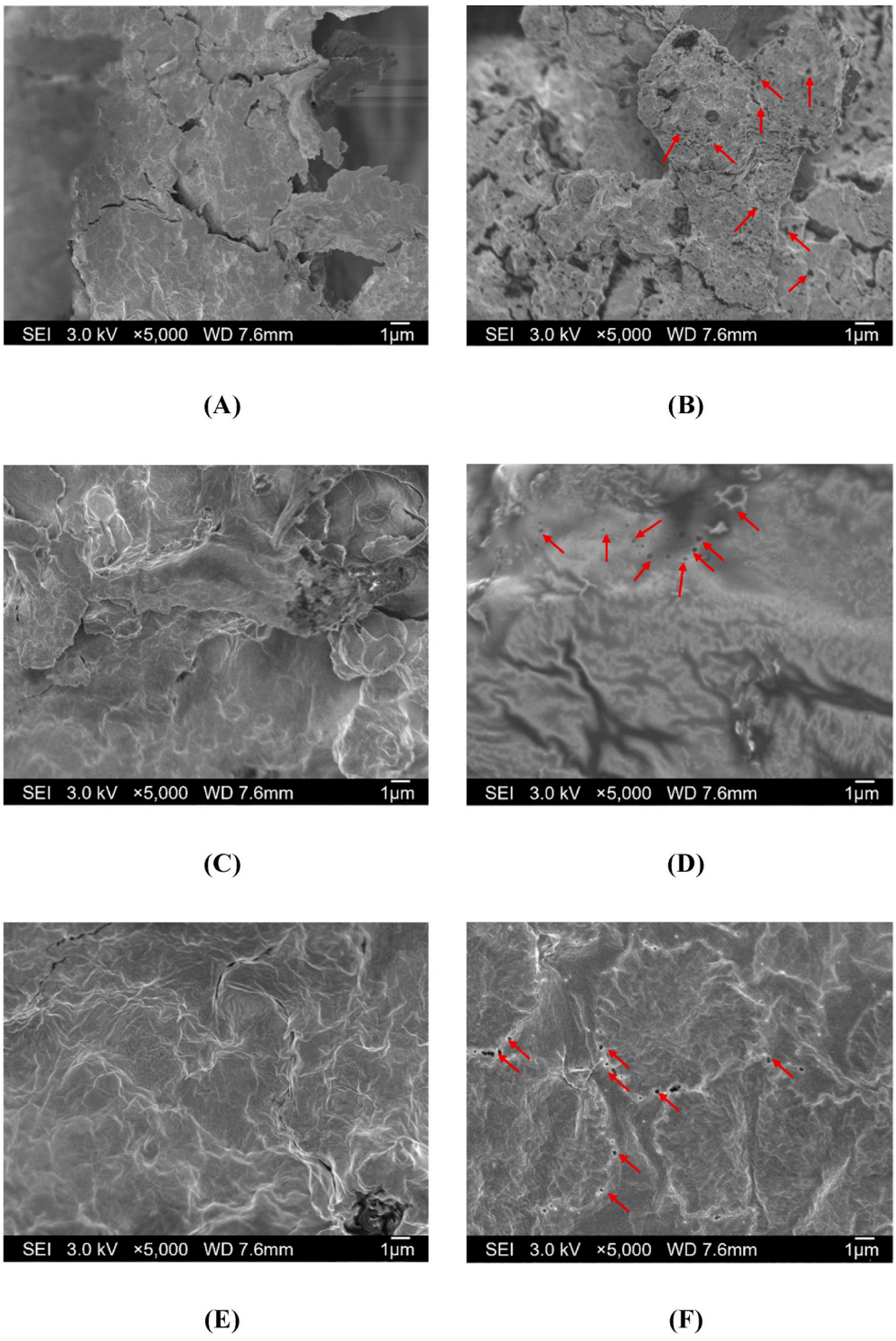

Fig. 7. The surface morphology for fishball (FB), plant-based fishball analogues (PFB). (A) and (B) The surface microstructure of FB before and after *in vitro* digestion, respectively; (C) and (D) The surface microstructure of PFB3.5 before and after *in vitro* digestion, respectively; (E) and (F) The surface microstructure of PFB6.5 before and after *in vitro* digestion, respectively; Note: PFB3.5 and PFB6.5 represent PFB at 3.5% and 6.5% konjac glucomannan addition, respectively.

irregular and less discontinuous structure than PFB6.5. Besides, some porous structures were formed in FB and PFB digesta (red arrows in Fig. 7). FB digesta had significantly more and larger pores than PFB digesta; meanwhile, PFB at higher KGM addition (PFB6.5) had fewer and smaller pores than PFB at lower KGM addition (PFB3.5). The formation of pores on the surface of digesta could be correlated with the enzymatic effect during digestion. Since KGM is a non-digestible polysaccharide, the pores in PFB digesta resulted from the breakdown of protein that did not incorporate with KGM. The decreased pores in PFB6.5 digesta indicated that KGM would promote the incorporation between SPI and KGM, providing fewer sites for enzymatic action and thus delaying the digestion of PFB. Hu et al. (2017) reported that the protein that did not combine with polysaccharides would firstly break down during digestion. Similarly, Huang et al. (2021) stated that many holes were found in the *in vitro* digesta of sponge cake formulated with *Eucheuma* powder.

4. Conclusions

Based on NMR-based foodomic profiling, a total of 27 metabolites were identified in PFB digesta after digestion, including amino acids, saccharides, fatty acids, and sterol. The obtained NMR spectra indicated that FB had an overall similar metabolite profile to PFB, although the content of individual metabolites was different. The observations from PCA and OPLS-DA models revealed that KGM at higher addition diminished the released metabolites after *in vitro* digestion process, possibly because KGM affected the metabolic pathways during digestion. Furthermore, FB digesta had a significantly lower yield stress τ_0 than PFB after *in vitro* digestion; in the meantime, PFB6.5 digesta had a significantly higher τ_0 value than PFB3.5 after digestion. Besides, KGM at higher addition also increased consistency index *K* (viscosity) and viscoelasticity G_0*, contributing to prolonging the digestion process and providing a satiety effect, which might help control blood glucose and cholesterol levels. Further sensory research may need to be conducted to confirm the satiety effect introduced by KGM. Overall, the present study helped a better knowledge of the metabolic changes and the rheological behavior of FB and PFB during *in vitro* digestion, revealing the impact of KGM on the digestive performance of PFB, which might contribute to developing more variety of plant-based seafood analogues containing KGM.

CRediT authorship contribution statement

Xinli Ran: Conceptualization, Methodology, Investigation, Software, Visualization, Validation, Writing – original draft, Writing – review & editing. **Zhixin Yang:** Methodology. **Yingfeng Chen:** Methodology. **Hongshun Yang:** Conceptualization, Funding acquisition, Project administration, Supervision, Writing – review & editing.

Declaration of competing interest

The authors declare that they have no known competing financial interests or personal relationships that could have appeared to influence the work reported in this paper.

Acknowledgments

We acknowledge the fund support from Applied Basic Research Project (Agricultural) Suzhou Science and Technology Planning Program (SNG2020061), Singapore Ministry of Education Academic Research Fund Tier 1 (R-160-000-A40-114), and an industry grant from Changzhou Wangxianglou Food Co., Ltd (R-160-000-B22-597).

Appendix A. Supplementary data

Supplementary data to this article can be found online at https://doi.org/10.1016/j.foodhyd.2022.107623.

References

Ahmed, J., & Ramaswamy, H. (2004). Effect of high-hydrostatic pressure and concentration on rheological characteristics of xanthan gum. *Food Hydrocolloids, 18*, 367–373.

Borderías, A. J., Tovar, C. A., Domínguez-Timón, F., Díaz, M. T., Pedrosa, M. M., & Moreno, H. M. (2020). Characterization of healthier mixed surimi gels obtained through partial substitution of myofibrillar proteins by pea protein isolates. *Food Hydrocolloids, 107*, 105976.

Bornhorst, G. M., Ferrua, M. J., Rutherfurd, S. M., Heldman, D. R., & Singh, R. P. (2013). Rheological properties and textural attributes of cooked brown and white rice during gastric digestion in vivo. *Food Biophysics, 8*, 137–150.

Cao, Q., Liu, H., Zhang, G., Wang, X., Manyande, A., & Du, H. (2020). ^{1}H-NMR based metabolomics reveals the nutrient differences of two kinds of freshwater fish soups before and after simulated gastrointestinal digestion. *Food & Function, 11*, 3095–3104.

Chen, H.-L., Cheng, H.-C., Liu, Y.-J., Liu, S.-Y., & Wu, W.-T. (2006). Konjac acts as a natural laxative by increasing stool bulk and improving colonic ecology in healthy adults. *Nutrition, 22*, 1112–1119.

Chen, L., Wu, J., Li, Z., Liu, Q., Zhao, X., & Yang, H. (2019). Metabolomic analysis of energy regulated germination and sprouting of organic mung bean (*Vigna radiata*) using NMR spectroscopy. *Food Chemistry, 286*, 87–97.

Chen, L., Zhao, X., Wu, J., He, Y., & Yang, H. (2020). Metabolic analysis of salicylic acid-induced chilling tolerance of banana using NMR. *Food Research International, 128*, 108796.

Dai, S., Jiang, F., Shah, N. P., & Corke, H. (2019). Functional and pizza bake properties of Mozzarella cheese made with konjac glucomannan as a fat replacer. *Food Hydrocolloids, 92*, 125–134.

Devaraj, R. D., Reddy, C. K., & Xu, B. (2019). Health-promoting effects of konjac glucomannan and its practical applications: A critical review. *International Journal of Biological Macromolecules, 126*, 273–281.

Escudero, E., Sentandreu, M. A.n., & Toldra, F. (2010). Characterization of peptides released by *in vitro* digestion of pork meat. *Journal of Agricultural and Food Chemistry, 58*, 5160–5165.

Ferranti, P., Nitride, C., Nicolai, M. A., Mamone, G., Picariello, G., Bordoni, A., et al. (2014). *In vitro* digestion of *Bresaola* proteins and release of potential bioactive peptides. *Food Research International, 63*, 157–169.

Fiszman, S., & Varela, P. (2013). The role of gums in satiety/satiation. A review. *Food Hydrocolloids, 32*, 147–154.

Funami, T. (2011). Next target for food hydrocolloid studies: Texture design of foods using hydrocolloid technology. *Food Hydrocolloids, 25*, 1904–1914.

Hayati, I. N., Man, Y. B. C., Tan, C. P., & Aini, I. N. (2009). Droplet characterization and stability of soybean oil/palm kernel olein O/W emulsions with the presence of selected polysaccharides. *Food Hydrocolloids, 23*, 233–243.

Herranz, B., Tovar, C. A., Borderias, A. J., & Moreno, H. M. (2013). Effect of high-pressure and/or microbial transglutaminase on physicochemical, rheological and microstructural properties of flying fish surimi. *Innovative Food Science & Emerging Technologies, 20*, 24–33.

Herranz, B., Tovar, C. A., Solo-de-Zaldívar, B., & Borderias, A. J. (2012). Effect of alkalis on konjac glucomannan gels for use as potential gelling agents in restructured seafood products. *Food Hydrocolloids, 27*, 145–153.

Huang, M., Zhao, X., Mao, Y., Chen, L., & Yang, H. (2021). Metabolite release and rheological properties of sponge cake after *in vitro* digestion and the influence of a flour replacer rich in dietary fibre. *Food Research International, 144*, 110355.

Hu, B., Chen, Q., Cai, Q., Fan, Y., Wilde, P. J., Rong, Z., et al. (2017). Gelation of soybean protein and polysaccharides delays digestion. *Food Chemistry, 221*, 1598–1605.

Hu, Y., Tian, J., Zou, J., Yuan, X., Li, J., Liang, H., et al. (2019). Partial removal of acetyl groups in konjac glucomannan significantly improved the rheological properties and texture of konjac glucomannan and κ-carrageenan blends. *International Journal of Biological Macromolecules, 123*, 1165–1171.

Iglesias-Otero, M. A., Borderías, J., & Tovar, C. A. (2010). Use of konjac glucomannan as additive to reinforce the gels from low-quality squid surimi. *Journal of Food Engineering, 101*, 281–288.

Jimenez-Colmenero, F., Cofrades, S., Herrero, A. M., Solas, M. T., & Ruiz-Capillas, C. (2013). Konjac gel for use as potential fat analogue for healthier meat product development: Effect of chilled and frozen storage. *Food Hydrocolloids, 30*, 351–357.

Keppler, S., O'Meara, S., Bakalis, S., Fryer, P., & Bornhorst, G. (2020). Characterization of individual particle movement during *in vitro* gastric digestion in the Human Gastric Simulator (HGS). *Journal of Food Engineering, 264*, 109674.

Kim, S. R. B., Choi, Y.-G., Kim, J.-Y., & Lim, S.-T. (2015). Improvement of water solubility and humidity stability of tapioca starch film by incorporating various gums. *LWT-Food Science and Technology, 64*, 475–482.

Kim, S.-K., & Van Ta, Q. (2012). Bioactive sterols from marine resources and their potential benefits for human health. *Advances in Food & Nutrition Research, 65*, 261–268.

Kumar, M. A., Bitla, A. R. R., Raju, K., Manohar, S. M., Kumar, V. S., & Narasimha, S. R. P. V. L. (2012). Branched chain amino acid profile in early chronic kidney disease. *Saudi Journal of Kidney Diseases and Transplantation, 23*, 1202.

Lentle, R., & Janssen, P. (2008). Physical characteristics of digesta and their influence on flow and mixing in the mammalian intestine: A review. *Journal of Comparative Physiology B, 178*, 673–690.

Li, J., Wang, Y., Jin, W., Zhou, B., & Li, B. (2014). Application of micronized konjac gel for fat analogue in mayonnaise. *Food Hydrocolloids, 35*, 375–382.

Liu, J., Chang, R., Zhang, X., Wang, Z., Wen, J., & Zhou, T. (2018). Non-isoflavones diet incurred metabolic modifications induced by constipation in rats via targeting gut microbiota. *Frontiers in Microbiology, 9*, 3002.

Lou, X., Zhai, D., & Yang, H. (2021). Changes of metabolite profiles of fish models inoculated with *Shewanella baltica* during spoilage. *Food Control, 123*, 107697.

Luo, X., He, P., & Lin, X. (2013). The mechanism of sodium hydroxide solution promoting the gelation of konjac glucomannan (KGM). *Food Hydrocolloids, 30*, 92–99.

Marcano, J., Hernando, I., & Fiszman, S. (2015). *In vitro* measurements of intragastric rheological properties and their relationships with the potential satiating capacity of cheese pies with konjac glucomannan. *Food Hydrocolloids, 51*, 16–22.

Minekus, M., Alminger, M., Alvito, P., Ballance, S., Bohn, T., Bourlieu, C., et al. (2014). A standardised static *in vitro* digestion method suitable for food - an international consensus. *Food & Function, 5*, 1113–1124.

Monirujjaman, M., & Ferdouse, A. (2014). Metabolic and physiological roles of branched-chain amino acids. *Advances in Molecular Biology*, 364976, 2014.

Morell, P., Fiszman, S., Varela, P., & Hernando, I. (2014). Hydrocolloids for enhancing satiety: Relating oral digestion to rheology, structure and sensory perception. *Food Hydrocolloids, 41*, 343–353.

Piras, C., Marincola, F. C., Savorani, F., Engelsen, S. B., Cosentino, S., Viale, S., & Pisano, M. B. (2013). A NMR metabolomics study of the ripening process of the Fiore Sardo cheese produced with autochthonous adjunct cultures. *Food Chemistry, 141*(3), 2137–2147.

Ran, X., Lou, X., Zheng, H., Gu, Q., & Yang, H. (2022). Improving the texture and rheological qualities of a plant-based fishball analogue by using konjac glucomannan to enhance crosslinks with soy protein. *Innovative Food Science & Emerging Technologies, 75*, 102910.

Rodriguez, L., Roberts, L. D., LaRosa, J., Heinz, N., Gerszten, R., Nurko, S., & Goldstein, A. M. (2013). Relationship between postprandial metabolomics and colon motility in children with constipation. *Neurogastroenterology & Motility, 25*(5), 420–e299.

Shah, B. R., Li, B., Wang, L., Liu, S., Li, Y., Wei, X., et al. (2015). Health benefits of konjac glucomannan with special focus on diabetes. *Bioactive Carbohydrates and Dietary Fibre, 5*, 179–187.

Shang, L., Wang, Y., Ren, Y., Ai, T., Zhou, P., Hu, L., et al. (2020). *In vitro* gastric emptying characteristics of konjac glucomannan with different viscosity and its effects on appetite regulation. *Food & Function, 11*, 7596–7610.

da Silva, D. F., de Souza Ferreira, S. B., Bruschi, M. L., Britten, M., & Matumoto-Pintro, P. T. (2016). Effect of commercial konjac glucomannan and konjac flours on textural, rheological and microstructural properties of low fat processed cheese. *Food Hydrocolloids, 60*, 308–316.

Van Vliet, S., Bain, J. R., Muehlbauer, M. J., Provenza, F. D., Kronberg, S. L., Pieper, C. F., et al. (2021). A metabolomics comparison of plant-based meat and grass-fed meat indicates large nutritional differences despite comparable Nutrition Facts panels. *Scientific Reports, 11*, 13828.

Wang, Y., Ning, Y., Yuan, C., Cui, B., Liu, G., & Zhang, Z. (2021). The protective mechanism of a debranched corn starch/konjac glucomannan composite against dyslipidemia and gut microbiota in high-fat-diet induced type 2 diabetes. *Food & Function, 12*, 9273–9285.

Wu, P., Dhital, S., Williams, B. A., Chen, X. D., & Gidley, M. J. (2016). Rheological and microstructural properties of porcine gastric digesta and diets containing pectin or mango powder. *Carbohydrate Polymers, 148*, 216–226.

Würtz, P., Soininen, P., Kangas, A. J., Rönnemaa, T., Lehtimäki, T., Kähönen, M., et al. (2013). Branched-chain and aromatic amino acids are predictors of insulin resistance in young adults. *Diabetes Care, 36*, 648–655.

Wu, J., Zhao, L., Lai, S., & Yang, H. (2021). NMR-based metabolomic investigation of antimicrobial mechanism of electrolysed water combined with moderate heat treatment against Listeria monocytogenes on salmon. *Food Control, 125*, 107974.

Yuan, C., Xu, D., Cui, B., & Wang, Y. (2019). Gelation of κ-carrageenan/konjac glucommanan compound gel: Effect of cyclodextrins. *Food Hydrocolloids, 87*, 158–164.

Zhang, Y.-q., Xie, B.-j., & Gan, X. (2005). Advance in the applications of konjac glucomannan and its derivatives. *Carbohydrate Polymers, 60*, 27–31.

Zhang, Q., Zhong, D., Ren, Y. Y., Meng, Z. K., Pegg, R. B., & Zhong, G. (2021). Effect of konjac glucomannan on metabolites in the stomach, small intestine and large intestine of constipated mice and prediction of the KEGG pathway. *Food & Function, 12*, 3044–3056.

Zhao, X., Chen, L., Wu, J., He, Y., & Yang, H. (2020). Elucidating antimicrobial mechanism of nisin and grape seed extract against *Listeria monocytogenes* in broth and on shrimp through NMR-based metabolomics approach. *International Journal of Food Microbiology, 319*, 108494.

Zheng, Y., Sun, W., Yang, W., Chen, S., Liu, D., Tian, J., et al. (2020). The influence of xanthan gum on rheological properties and *in vitro* digestibility of Kudzu (*Pueraria lobata*) starch. *Starch - Stärke, 72*, 1900139.